
Article:
Leonardi, A. orcid.org/0000-0002-7900-8376, Pirulli, M., Barbero, M. et al. (5 more authors) (2021) Impact of debris flows on filter barriers : analysis based on site monitoring data. Environmental and Engineering Geoscience, 27 (2). pp. 195-212. ISSN 1078-7275

https://doi.org/10.2113/eeg-d-20-00013

General information of the article
Type of paper: Original research paper
Title: Impact of debris flows on filter barriers: analysis based on site monitoring data

Authors: A. Leonardi, M. Pirulli, M. Barbero, F. Barpi, M. Borri-Brunetto, O. Pallara, C. Scavia, V. Segor.

Author information:
Corresponding author: Alessandro Leonardi
Post-doctoral Fellow, Department of Structural, Geotechnical and Building Engineering, Politecnico di Torino, Corso Duca degli Abruzzi 24, 10129 Turin, Italy.
E-mail: alessandro.leonardi@polito.it

Co-author: Marina Pirulli
Associate Professor, Department of Structural, Geotechnical and Building Engineering, Politecnico di Torino, Corso Duca degli Abruzzi 24, 10129 Turin, Italy.
E-mail: marina.pirulli@polito.it

Co-author: Monica Barbero
Associate Professor, Department of Structural, Geotechnical and Building Engineering, Politecnico di Torino, Corso Duca degli Abruzzi 24, 10129 Turin, Italy.
E-mail: monica.barbero@polito.it

Co-author: Fabrizio Barpi
Associate Professor, Department of Structural, Geotechnical and Building Engineering, Politecnico di Torino, Corso Duca degli Abruzzi 24, 10129 Turin, Italy.
E-mail: fabrizio.barpi@polito.it

Co-author: Mauro Borri-Brunetto
Associate Professor, Department of Structural, Geotechnical and Building Engineering, Politecnico di Torino, Corso Duca degli Abruzzi 24, 10129 Turin, Italy.
E-mail: mauro.borri@polito.it

Co-author: Oronzo Pallara
Laboratory manager, Department of Structural, Geotechnical and Building Engineering, Politecnico di Torino, Corso Duca degli Abruzzi 24, 10129 Turin, Italy.
E-mail: oronzo.pallara@polito.it

Co-author: Claudio Scavia
Full professor, Department of Structural, Geotechnical and Building Engineering, Politecnico di Torino, Corso Duca degli Abruzzi 24, 10129 Turin, Italy.
E-mail: claudio.scavia@polito.it

Co-author: Valerio Segor
Director, Direzione Assetto Idrogeologico dei Bacini Montani, Aosta Valley Autonomous Region, Loc. Amerique 33, 11020 Quart, Italy.
E-mail: v.segor@regione.vda.it

Number of words in abstract: 205
Number of words in main text: 8794
Number of tables: 5
Number of figures: 13

Impact of debris flows on filter barriers: analysis based on site monitoring data

A. Leonardi[1], M. Pirulli[1], M. Barbero[1], F. Barpi[1], M. Borri-Brunetto[1], O. Pallara[1], C. Scavia[1], V. Segor[2].

[1]Department of Structural, Geotechnical and Building Engineering, Politecnico di Torino, Italy
[2]Direzione Assetto Idrogeologico dei Bacini Montani, Aosta Valley Autonomous Region, Aosta, Italy

Abstract

Debris flows are one of the most complex and devastating natural phenomena, and they affect mountainous areas throughout the world. Structural measures are currently adopted to mitigate the related hazard in urbanized areas. However, their design requires an estimate of the impact force, which is an open issue. The numerous formulae proposed in the literature require the assignment of empirical coefficients, and an evaluation of the kinematic characteristics of the incoming flow. Both are generally not known a priori.

In this paper, we present the Grand Valey torrent site (Italian Alps). A monitoring system made up of strain gauges was installed on a filter barrier at the site, allowing the evaluation of impact forces. The system provides pivotal information for validating calibrating impact formulae.

Two debris flows occurred during the monitoring period. We present the interpretation of videos, impact measurements, as well as the results of numerical analyses. The combined analysis allows a back-calculation of the events in terms of forces, flow depth and velocity. Thus, we investigate the applicability of the impact formulae suggested in the literature, and of the recommended empirical coefficients. The results highlight that hydrostatic effects dominated the impact during the first event, while hydrodynamic effects prevailed in the second one.

Keywords: debris flows, structural mitigation measures, impact forces, site monitoring system, numerical modelling

Introduction

Debris flows are extremely rapid flow-like landslides that involve a mixture of fine (clay, silt and sand) and coarse (gravel, cobbles and boulders) materials with a variable quantity of water. Their high velocity, impact force, and long runout, combined with poor temporal predictability, make them a major source of hazard for human life and activities in mountainous regions. They cause severe damage and casualties throughout the world each year (Guzzetti *et al.*, 2005; Hilker *et al.*, 2009; Jakob *et al.*, 2012; Dowling & Santi, 2014). As a consequence, countermeasures are usually adopted to mitigate the related risk.

Concrete dams are among the possible interventions. These are often complemented with drainage filters (filter barriers). The filters are used for the retention of large boulders (which have a high destructive potential), while allowing water and smaller-sized particles to flow through (Marchelli *et al.*, 2020). However, an estimate of impact forces is needed for a reliable design of these structures.

Typically, the impact force is estimated as either a function of the hydrodynamic pressure exerted by the fluid, assumed in steady conditions (e.g. Armanini & Scotton, 1993; Daido, 1993; Canelli *et al.*, 2012) or as a function of the hydrostatic load (e.g. Lichtenhan, 1973; Armanini, 1997). Both these formulations require the selection of empirical coefficients, and knowledge of the flow dynamics before impact (i.e. flow depth and front velocity). The determination of empirical coefficients is particularly critical: multiple sets of recommendations, often conflicting, can be found in the literature (e.g. Huang *et al.*, 2007).

A contribution to the knowledge of the debris flows dynamics before impact may be obtained, to a certain extent, through numerical modelling (e.g., Iverson & Denlinger, 2001; Pitman & Le, 2005; Pudasaini *et al.*, 2005; Pirulli, 2005). However, the accuracy of the results depends on the quality of the rheological parameters plugged in the model (Pirulli, 2010a), whose calibration can only be achieved through measurement and observation of events.

Physical modelling of flows in laboratory small- or medium-scale channels (e.g. Armanini & Scotton, 1992; Iverson *et al.*, 2004, 2010; Canelli *et al.*, 2012; Hürlimann *et al.*, 2015) allows the phenomenon to be investigated under controlled conditions. However, the obtained results are affected by scaling issues, and problems arise concerning the representativeness of the flow composition with respect to site conditions. Data from real events would allow this limitation to be overcome. However, the number of monitored sites is still limited, especially due to the cost and complexity of the logistics.

Examples of instrumented sites are those of China (Okuda *et al.,* 1980; Zhang 1993; Suwa *et al.,* 2011), the United States (Pierson 1986; Coe *et al.,* 2008; McCoy *et al.,* 2010), Taiwan (Yin *et al.,* 2011), France (Navratil *et al.,* 2012, 2013), Austria (Kogelnig *et al.,* 2014), Italy (Arattano *et al.,* 1997; Berti *et al.,* 1999; Marchi *et al.,* 2002; Comiti *et al.,* 2014), Spain (Hürlimann *et al.,* 2011)

and Switzerland (Hurlimann *et al.,* 2003; McArdell *et al.,* 2007; Berger *et al.,* 2011). Unfortunately, only few of these sites monitor the flow dynamics and measure the impact on a mitigation structure at the same time. An example of such a case is the Illgraben monitoring site in Switzerland (Wendeler *et al.,* 2006), where a flexible ring net barrier is monitored by means of load cells, or that of Erill in the Spanish Pyrenees (Luis-Fonseca *et al.,* 2011). Strain sensors have been installed on a 2.5 m high steel pile foundation located in the middle of the Jiangjia Ravine channel in China (Hu *et al.,* 2011). An experimental set-up that integrates a video camera, radar, ultrasonic and load cells in a 1.6m high target has been installed in the middle of the Schesatobel watershed in Austria (Kaitna *et al.*, 2007). Nevertheless, to the best of our knowledge, no instrumented site exists where impact forces of debris flows are measured directly on the elements of a real rigid barrier and a video of the flow dynamics is contemporaneously recorded.

In this work, we present a monitored site, where a video of the flow dynamics and the interaction with a monitored barrier is available together with a direct measurement of impact forces. This is the Grand Valey torrent site (North-Western Italian Alps, the Aosta Valley Autonomous Region). There, a monitoring system, made up of strain gauges, is installed on the filter elements of a barrier. The measured strain gauge deformations are converted into forces, assuming linear elastic behavior of the barrier filter elements. The site is characterized by an annual frequency of events and by the existence of a set of debris-flow control structures. Two debris flows occurred during the monitoring period considered here.

The flow dynamics before impact are reconstructed by means of RASH3D, a code based on a continuum-mechanics approach. The back-analysis of the first event allows the rheological parameters of the model to be calibrated on the basis of the available video information. The parameters are then used to simulate the second event, for which less information is available. While the code is not suited to simulate three-dimensional fluid-structure interaction accurately, it allows to quantitatively estimate values of flow height and velocity before impact, which can be plugged into a set of formulae that estimate impact forces. Thus, we are able to back-calculate the empirical coefficients. The obtained results are then compared with the range of values suggested in literature and we comment on their applicability to the Grand Valey study case.

Description of the Grand Valey test site

The Grand Valey site is located in the municipality of Saint-Vincent, a small town in the central part of the Aosta Valley Autonomous Region, North-West Italy (Fig. 1a).

Morphology and geology

The basin, which is delimited in the upper part by Mount Zerbion (2730 m a.s.l.) and Mount Je Tire (2141 m a.s.l.), has a drainage area of 5.22 km^2 and it extends from 2681 m to 680 m a.s.l., with

a mean slope of 82%. The alluvial fan instead extends for 1.47 km^2, from 680 m to 445 m a.s.l. (Fig. 1a and Table 1).

The middle-upper part of the basin consists of sub-vertical slopes of schists, characterized by a high degree of fracturing and poor vegetation, with subordinate phyllitic layers, serpentinite, and greenschist metagabbros. In the lower part, towards the apex area of the alluvial fan, these rock types are interbedded with layers of Austroalpine nappe, both on the left and on the right banks.

In this context, the Grand Valey torrent extends for 5.71 km from its origin at 2681 m a.s.l. to the confluence with the Dora Baltea river, the main river in the Aosta Valley, at 445 m a.s.l.. The torrent flows for 3.76 km in the aforementioned basin with a mean slope of 38%, which decreases to 12% along the 1.95 km of the fan (Fig. 1a).

The upper part of the torrent divides into two main branches, which have an estimated total length of 14.76 km: the first one comes from southern slopes (A in Fig. 1) of Mount Zerbion (2730 m a.s.l.) while the second one (B in Fig. 1) originates from Mount Je Tire (2141 m a.s.l.). These two branches are in turn composed of two sub-branches (A1, A2, B1, B2 in Fig. 1), which are oriented according to the main discontinuities of the rock mass. All the flow directions merge into a single channel at 1075 m a.s.l. at Pèrriere (Fig. 1), which is located upstream of the experimental site and of the urbanized area of Saint Vincent. The morphological features are summarized in Table 1.

Debris flow activity and undertaken mitigation countermeasures

The upper part of the Grand Valey basin is affected by large and continuous rock fall phenomena, due to the steep slopes and to the high fracturing of the overhanging rock mountain faces. Site surveys identified branch A2 from the Mount Zerbion and branch B1 from Mount Je Tire as the main sources of rock debris (Fig. 1b). Each year, during heavy rains in spring and summer, debris is transported downstream by debris flows (Table 2). The B1 channel is only activated during the most intense rainfall events.

The regional government has improved and increased the number of defensive structures located along the torrent to reduce consequences on the urbanized area below. However, no countermeasures have been set up in the upper part of the basin because of the difficulty in reaching and stabilizing the coarse material on the steepest slopes.

At present, the protection system, from upstream to downstream, consists of two filter barriers, positioned about 46.5 m from each other, at the Pèrriere hamlet (1075 m a.s.l) (indicated as 1 in Fig. 1 and detailed in Fig. 2a), which together can retain up to 5000 m^3 of material, two steel-net barriers (indicated as 2 in Fig. 1 and detailed in Fig. 2b) and one slit-filter barrier (indicated as 3 in Fig. 1 and detailed in Fig. 2c) located at the Tromen hamlet (700 m a.s.l.). After each debris flow event, the material retained by the filter barriers is rapidly removed by maintenance workers in order to restore the complete functionality of the mitigation system.

In the event on 20 July 2014 (Table 2), the first filter barrier at Pèrriere (Fig. 2a in the white rectangle), located immediately downstream of the confluence of branches A and B, collapsed (Fig. 2d). This barrier was the first to be impacted during events. The barrier was reconstructed at the same position in 2015 (Fig. 2a, white box). The lower part of the new barrier is a 17 m long, 1.15 m thick and 2.55 m high reinforced concrete wall. A 12 m width rack, made up of eighteen IPE 270 steel beams (Euronorm 19-57), with a nominal spacing of 0.6 m, is placed on the upper side of the concrete wall to form a filter (Figs. 3a-3b). The steel beams are 3.0 m long and are embedded into the concrete structure for a length of 1.0 m (Fig. 3c).

The debris flow activity is very frequent (Table 2) and the area has easy access. For these reasons, the site was selected, in 2012, for the installation of a monitoring station. The monitoring system quantifies the deformation of the steel beams that constitute the filter. On the barrier that was reconstructed in 2015 the monitoring system was re-installed and upgraded (Pirulli *et al.*, 2014).

Configuration of the monitoring system

The monitoring system consists of several Hottinger Baldwin HBM SLB-700A strain sensors. These devices are designed to measure the deformations of the structural parts on which they are mounted (Fig. 3d). They consist of a metallic box that contains four electric strain gauges, connected to form a Wheatstone bridge, which reacts to the axial dilation or contraction of the instrument by varying their electrical resistance. The transducers operate effectively across a temperature range of -20 °C to 60 °C, and automatically compensate for thermal expansion. When properly powered and controlled, the devices provide the local axial strain of the structure up to a nominal strain of ±500 μm/m, which is proportional to the measurement of the voltage variation of the Wheatstone bridge (nominal sensitivity 1.5±0.15 mV/V). The presence of these transducers slightly affects the strain at the installation point, but the perturbation of the measurements can be accurately evaluated to obtain the correct strain value (Borri-Brunetto *et al*., 2016).

In the Pèrriere site, 20 strain sensors (indicated as "E + strain gauge number" in Fig 3a) are installed on the downstream flange of the IPE270 steel beams: 18 of them are positioned at the lower right corner of each steel beam and 2 additional are located at mid-height of the two central steel beams (Fig. 3a). Each transducer is mounted at an average distance of 140 mm from the concrete wall on which the beams are embedded. Each strain transducer is protected against water and the impact of solid material by a steel box (Fig. 3d). Each steel box is welded to the beam, but only along its upper side, to exclude local stiffening effects due to the box itself, and is waterproofed by silicone sealing and a two-component sealant gel filling.

The strain transducers are connected to a Compact FieldPoint (National Instruments cFP-2220) programmable controller equipped with three different eight-channel input modules with 16-bit resolution (National Instrument cFP-SG-140) (Fig. 3e). The controller acquires the strain

measurements from the transducers at time intervals of 1.15 s (0.87 Hz) and stores data every 10 minutes on a removable solid-state drive. The software controlling the Compact FieldPoint was developed within the National Instruments LabVIEW programming environment.

The controller is placed, near the barrier, inside a waterproof container protected with a stainless-steel locker (Fig.3f). Electric power is supplied by an underground cable that runs from the monitoring site to the Pèrriere hamlet, but an uninterruptible power supply (UPS) is installed to cope with power cuts. A grounding wire protects from damage caused by thunderstorms (Fig. 3e).

The 2016 debris flows

Two main debris flows occurred in the Grand Valey after the monitoring system was installed on the reconstructed barrier: on 9 June (Fig. 9a) and 11 July (Fig. 10a). The mass mobilized in both events was retained almost completely by the two filter barriers at Perrière. For this reason, the estimation of the involved volumes was made on the basis of the material removed from the basins after each event.

Fig. 4 shows the rainfall data recorded by the weather station located in Saint-Vincent Terme (Fig. 1a). The two events were triggered by rainfall events that had different characteristics in terms of both intensity and duration. The first and second events were triggered by precipitations with a one-year and two-year return period, respectively. In both cases, the recorded rainfall is lower than the typical threshold for this region (around 20 mm/h, see Tiranti *et al*., 2014). However, the weather station is located about 2900 m away from the site, and at a lower elevation (626 m a.s.l.), and is only a poor indicator of the actual hydrological conditions on the upper catchment.

The debris flow on 9 June occurred at about 12:38 (UTC). In addition to strain sensors, a set of amateur videos of this event is available, since technicians were working at the Pèrriere barrier at that time. Eyewitness reports and post-event site surveys confirm that the event consisted of one surge that originated from branch A2 (Fig. 1a-b). The mass deposited principally upstream of the monitored barrier and assumed an approximately trapezoidal shape in plan view, whose main dimensions are summarized in Table 3. Operation for removal of the deposit allowed (i) estimation of the retained volume to about 1875 m^3 and (ii) excavation of a longitudinal trench through the deposit that highlighted a grain-size distribution with inverse grading of the clasts with respect to maximum clast size (Fig. 5), and the average depth distribution as summarized in Table 3 and Fig. 11e.

The debris flow on 11 July occurred at about 16:00 (UTC). Although no videos or detailed measurement of the deposit are available for this event, an on-site survey indicated that flows traveled down branches A and B (Fig. 1). Both the upstream and the downstream retention basins at Pèrriere filled completely, but a different type of material caused clogging of the two barriers: rock blocks clogged the upstream barrier, while woody debris (driftwood) clogged the downstream one

(Fig. 6). The technical staff of the Aosta Valley Autonomous Region, which is in charge of regular on-site inspection of the area, reported that driftwood usually comes from branch B, which is only active during major rainfall events (Fig. 4b).

A first interpretation of the flow dynamics is as follows: a first surge came from branch A and probably caused the clogging of the first barrier, while a second surge, transporting woody debris from branch B, occurred within a few hours from the first one. The second surge flowed over the deposit left by the first surge on the first retention basin. It then deposited in the second retention basin, before the second barrier.

During the debris removal operations, the total volume of debris deposited in the Pèrriere basins was estimated to be about 4420 m^3. A visual analysis of the deposit notes that the clasts entrained and transported during the event on 11 July were on average larger than those mobilized during the event on 9 June. With the exception of the largest clasts, the grain-size distribution with inverse grading resulted approximately the same for the two events.

Dynamics of the event on 9 June 2016 based on video analysis

Although the available videos of the event on 9 June are amateur, they are sufficient to reconstruct the process dynamics. The flow can be tracked from the moment the front reaches the confluence between branches A and B to when it stops moving. The main process of debris displacement lasted about 3 minutes (from 12:38 to 12:41), while the water flow lasted longer.

The flow front, at an early stage, featured a large number of coarse grains that were pushed upward and forward by a finer-grained matrix (Fig. 7a). The left side of the flux then rapidly assumed a more fluid-like behaviour with coarse particles in suspension. The blocks mainly concentrated on the right side, and advanced more slowly (Fig. 7b). At the interaction with the first barrier at Perrière, the asymmetric front caused a rapid obstruction of the right part of the barrier filter, while the left part was loaded dynamically by the passage of the fluid for a longer time (Fig. 7c). In the final stage, the whole process was characterized by a diluted flow that caused the deposition of a thin muddy veneer (Fig. 7d).

The video analysis of the time necessary for the front to cover the distance between the confluence between branches A and B and the first impacted barrier gives an estimated average front velocity of about to 2 m/s. Furthermore, frame extraction and particle tracking from the available videos allow an estimate the flow velocity at impact, as illustrated in Fig. 8. A systematic use of particle-tracking velocimetry (PTV) is possible. However, because of the low quality of the video, obtaining a consistent velocity field is difficult. Therefore, we focus on estimating the velocity from a set of clearly-visible particles distributed on the flow surface (Table 4). From these, an average velocity of about 2 m/s is estimated.

In the following sections, we interpret the measurements from the strain transducers. We also conduct a numerical modelling of the two events that occurred to carry out an in-depth analysis of the flow dynamics and gather all the information necessary to evaluate the applicability of literature impact formulae. We finally test whether the back-calculated empirical coefficients are within the range suggested in literature.

Analysis and interpretation of the strain measurements

The 20 strain transducers installed on the steel beams measure the axial deformation induced by flow impact. Due to the position of the instruments, a negative strain indicates a compressed gauge, while a positive strain indicates a tensed gauge. Negative values can also be induced by a lateral bending of the beam. This can happen when the outlet between two beams is clogged by rock blocks, which then load the two beams transversely with respect to the flow direction. Since the strain gauges are in the lower right corner of the steel beams (Fig. 3a), in this situation one transducer will be compressed (negative strain) and the other will be tensed (positive strain). This scenario has been tested and successfully back-calculated though discrete-element simulations by Leonardi & Pirulli (2020).

The event on 9 June 2016

The interpretation of the strain transducer recordings is supported by the amateur videos of the event on 9 June. During this event, strain gauges E14 and E18 were unresponsive. By comparing video and strain recordings, we observe four signal patterns, grouped in different panels in Fig. 9. Panel (b) and (d) group the majority of the signals coming from the right (E01-E10) and from the left (E11-E20) sides of the barrier, respectively. The signals from the left (panel b) show no evidence of an impulsive signal. From the video recordings, we see that in this area the flow reached the barrier at low velocity and progressively loaded the barrier (black horizontal arrow). Conversely, the signals from the right side (panel d) reflect a more fluid-like and turbulent behavior (as in Leonardi *et al.*, 2019), due to the flow transiting for a longer time on this side with more energy.

Panels (c) and (e) show instruments that recorded strong signals, which are induced by large blocks that clogged the outlets, loading transversely the beams.

The event on 11 July 2016

The measurements of the strain transducers confirmed the multi-surge nature of the event on 11 July, and the impulsive behavior of these surges (Fig. 10). Although no video recordings are available, the high values of the strain peaks in the recordings of this event indicate a higher-energy process compared to the event on 9 June.

As for the event on 9 June, signals that report similar patterns are grouped together and shown in panels in Fig. 10. Three main perturbations (surges) are recorded at about 16:00:46, 16:02:18 and 16:06:08. With few exceptions, the surges can be identified in all recordings reported in the figure. Each surge is characterized by a sudden strain increment (impulsive behavior), and is preceded by a variable time interval in which strains remain roughly constant (shaded areas in the figure). A rough indication of the initiation of each surge is shown by the horizontal numbered arrows in panel (c). The strains, are generally larger than those recorded on 9 June.

Numerical modelling of the flow dynamics

An indication of flow depth (h) and velocity (v) is a necessary input for using impact force formulae. As a consequence, their knowledge is needed to evaluate the applicability of the formulae to this case study.

The aim of the numerical analysis is to calibrate the rheological parameters of the model through a back analysis of the event on 9 June. The propagation analysis is carried out with RASH^{3D}, a numerical code based on a single-phase integrated solution of the St. Venant equations using the shallow-water assumption. The equations are solved with a finite-volume approach, where the CFL condition has been imposed to define the time discretization. An unstructured triangular mesh is used to discretize the equations. Full details concerning the code formulation and implementation are presented in Audusse *et al.,* (2000) and Pirulli (2010b). The calibration is achieved through a trial-and-error process by systematically modifying the parameters until the characteristics of the simulated phenomenon match those of the real event.

The numerical code, being based on a depth-integrated version of the balance equations, can only roughly simulate fluid-structure interaction. To obtain a clear representation of interaction, and of the complex three-dimensional flow that develops at impact, more sophisticated methods are required (possibly grain-resolving, as in Leonardi & Pirulli, 2020). However, RASH^{3D} can reasonably reproduce the main flow features until a few instants before impact. This is in terms of average flow depth and velocity before the impact with the Pèrriere barrier (obtained from the video analysis) and depth distribution of the deposited mass upstream of the barrier (observed along the longitudinal trench excavated during the deposit removal works). Under the hypothesis of the two events having a similar rheological behavior, the calibrated rheological parameters for the event on 9 June are used to model the event on 11 July and interpret its dynamics, since no videos are available.

Scenario and rheological law definition

In order to run an analysis, RASH3D requires: (i) a Digital Elevation Model (DEM), (ii) the geometry of the initiation volume and (iii) a rheological law.

A pre-event DEM with a 5 m grid spacing in both directions (based on 1:5000 maps) is available for the considered study site. The mesh grid is locally refined at the location of the barrier, down to a mesh spacing of 0.1 m. The filter barrier is included in the topography by locally modifying the DEM, albeit with a few simplifications (e.g. the I-shape of the beam section is not represented). For the event on 9 June it is assumed that the debris was released only from Area 1. For the event on 11 July a simultaneous release from both areas (i.e. Area 1 + Area 2) is considered.

RASH^{3D} can simulate entrainment with the model of McDougall & Hungr (2005). However, in St. Vincent the debris are mobilized from the steep slopes of the upper catchment (Area 1 and Area 2), and no significant entrainment is observed during the early runout on branches A and B. For this reason, no entrainment along the runout path is considered in the numerical analysis. The initiation volume of each scenario is therefore assumed equal to the volume removed during the works conducted to restore the functionality of the Périere mitigation barriers: 1875 m^3 for the event on 9 June and 4420 m^3 for the event on 11 July.

Different rheological parameters have to be defined as a function of the selected rheological law. In this work, we employ the Voellmy rheology. This law assumes that dissipation of kinetic energy is due to a combination of frictional resistance and of a turbulent-viscous drag term (Rickenmann & Koch, 1997; Revellino *et al.*, 2004, Rickenmann, 2005; Pirulli, 2010c, Pirulli & Marco, 2010; Pirulli & Pastor, 2012). Thus, the basal resistance T can be written as:

$$T = \rho g h \mu + \rho g \frac{v^2}{\xi} \qquad [1]$$

where, μ is the friction coefficient, ρ is the material density, g is gravity, and ξ is the turbulence coefficient. The two dependent variables are the depth averaged flow velocity v and the flow height h. The first term on the right side of equation [1] accounts for any frictional component of resistance. The second term is analogous to the Chezy formula for turbulent flows in open channels. In this case, it is included to empirically account for all possible sources of velocity-dependent resistance.

Results

The event on 9 June is back-analyzed to calibrate the two Voellmy parameters: the friction coefficient, μ, and the turbulence coefficient, ξ. The starting values were obtained from technical literature (e.g. Revellino *et al.*, 2004; Rickenmann *et al.*, 2006). The investigated range is as follows: friction coefficient between 0.1 and 0.2, and turbulence coefficient between 100 and 1000 m/s^2. Comparison of numerical results with average observed data are summarized in Table 5. Note that simulations with a higher friction coefficient tend to produce longer deposits, because the angle of the repose of the material increases as well. The best fit results were obtained for μ = 0.2 and ξ = 500 m/s^2, and are illustrated in Fig. 11.

The best-fit numerical results and the data obtained from the video recordings exhibit a good correlation on the runout reach above the monitored barrier. The front travels a distance of about 80 meters (from the confluence between branches A and B to the monitored barrier) in about 40 seconds. In this area, the computed mean velocity of the flow front, obtained averaging over the first 10 meters of moving debris, is about 2 m/s. This is close to the value obtained from the video analysis (Table 4).

Numerically, the flow depth at initial impact ranges from 0.2 m to 0.4 m (Fig. 11a). This was however immediately followed by the arrival of more debris, leading to a flow height of about 0.6-0.8 m. This does not exactly match the video, although a flow depth of about 0.6 m was observed in the video. After impact, the debris accumulate behind the barrier (Fig. 11b). Once the accumulated debris reach the top of the concrete basement, some material filters through the gaps between the vertical bars, further traveling along the channel (Fig. 11f). With respect to the final deposit, the computed configuration shows an average depth of about 2.5 m for the portion close to the barrier (Fig. 11g). The depth decreases progressively upstream.

Under the hypothesis of the two debris flows having similar rheological behavior, the calibrated rheological parameters are used to simulate also the event on 11 July, for which no video is available. In this case, the numerical analyses yield a front speed of about 4 m/s before impact. An interesting aspect that emerges is that, even though the material is released simultaneously from Area 1 and Area 2, the flow from Area 2 is delayed compared to that from Area 1. This behavior is in agreement with the interpretation from the site surveys. A first surge from Area 1 probably caused the clogging of the first barrier. After about 300 s, a successive surge, transporting woody debris, arrived from Area 2 soon after the first event, and flowed over the deposit in the retention basin (Fig. 12).

Estimation of the impact force

Since the monitored barrier is almost perfectly orthogonal to the Gran Valey channel, and the flowing mass is confined by the channel, it is reasonable to assume (as confirmed from the video recordings) that the impact of the flowing mass is orthogonal to the barrier. Thus, we assume here that the impact induces a simple uniaxial bending of the filter beams. While this simplification allows to capture the key aspects of the problem, the actual interaction mechanism is likely more complex. For example, the beams can also potentially bend laterally due to grains interlocking at the outlets, as shown by Leonardi & Pirulli (2020).

Assuming that deformations are within the elastic limit, a cantilever beam model with a uniform distributed load (q) over the beam length (l) can be used to determine the actual bending moment M_x induced in the cross-section a-a of the beam. The cantilever beam is 2 m long. Its section is an IPE270 profile with a deflection resistance modulus W_x equal to 428.900 mm^3 and a Young modulus (E) of 200.000 MPa. The length (l) of the distributed load can be assumed to be the depth

of the flow front. The a-a cross-section on which M_x is computed is centered on the strain transducer, which is at a known distance a from the beam fixed constraint. Under this load configuration, the axial strain (ε_z) of the beam measured by the strain transducer results in:

$$\varepsilon_z = \frac{\sigma_z}{E} = \frac{M_x}{EW_x} = \frac{q(l-a)^2}{2EW_x}, \quad [2]$$

which solved with respect to q, yields an impact force F of:

$$F = q \cdot l = \frac{2EW_x\varepsilon_z}{(l-a)^2} \cdot l. \quad [3]$$

The solution of the above equation requires however a knowledge of the impact depth of the flow (l), which can either come from the video recordings, or from the calibrated simulations. By comparing videos and strain recordings it is possible to define the flow depth that led to the peak deformations of the event on 9 June; this value was found to be about 1.0 m and was recorded at about 12:39 (UTC). The same flow depth of 1.0 m is assumed for the event on 11 July, since no videos are available. This value is clearly an approximation, but it can be used to compare the maximum impact force induced by the two events under similar conditions.

The forces derived from the strain measurements are then expressed dimensionally as a force per unit width. Obtained results are summarized in Fig. 13 for the two events. It emerges that the maximum impact force is due to compression of the transducers. The tension value is usually small except for the steel beams located at the dam side for the event on 11 July.

The mean impact force recorded for the event on 11 July (365.38kN/m) (Fig. 13b) is as much as 5.5 times greater than that of the event on 9 June (66.40kN/m) (Fig. 13a). It can be observed that there is a narrow distribution of values for the 9 June event and a wide distribution for the 11 July event .

Comparison with literature impact formulae

Several formulae exist in the literature to estimate the impact force on a rigid barrier. These can be grouped into two main families. The first is typical of slow flows and is based on a pressure term (hydrostatic models), while the second type is characteristic of rapid flows and is computed on the basis of the incoming flow momentum (hydrodynamic models).

Generally, hydrostatic formulae have the appearance:

$$F_s = \frac{1}{2}k\rho g h^2, \quad [4]$$

where F_s is the hydrostatic impact force, with k the empirical static coefficient. Lichtenhahn (1973) proposes k-values between 7 and 11 and Armanini (1997) proposes a value of 9.

Hydrodynamic formulae, usually take the form:

$$F_d = \alpha \rho h v^2 \qquad [5]$$

where F_d is the hydrodynamic impact force and α is the empirical dynamic coefficient. The range of values for the dynamic coefficient is in general larger than for the static coefficient. Armanini and Scotton (1993) propose values of α between 0.7 and 2. Canelli *et al.,* (2012) define α in a range between 1 and 5. Daido (1993) suggests values between 5 and 12.

The estimation of k and α remains an open issue. For this reason, these formulae have been used here to verify whether the literature coefficients are suitable for reproducing the impact forces of the Grand Valey debris flows, and in particular the values computed in the previous section (Fig. 13). In any case, the results are not to be interpreted as general recommendations, because they rely on multiple assumptions both on the flow features and on the structural behavior of the barrier.

To back-calculate the coefficients, we use the flow depth (h) and velocity (v) obtained from the video analysis (h = 1 m; v = 2 m/s) for the event on 9 June. For the event on 11 July, the velocity obtained from the numerical analysis is used (v = 4 m/s), while the flow depth is assumed equal to 1 m. The bulk density is assumed equal to 1900 kg/m^3. The results are shown in Figs. 13c and 13d, respectively, for both the single beam and as an average for both events. For the static coefficient k, a mean value equal to 10.6 was obtained for the event on 9 June, and equal to 39.0 for the event on 11 July. Only the first of these values falls inside the range proposed in the literature, which seem to confirm that the hydrostatic approach is more appropriate for slower impacts, such as those measured on 9 June. There is a small dispersion of results for the event on 9 June and a wide dispersion for the event on 11 July (Fig. 13c).

For the dynamic coefficient α, a mean value equal to 9.8 was obtained for the event on 9 June, and equal to 11.5 for the event on 11 July. Both the values fall only in the range proposed by Daido (1993). In this regard, it should be pointed out that Daido is the only author, among those selected, who uses real cases and not laboratory experiments. Moreover, even if the two mean values are close, the dynamic coefficient shows a wider dispersion for the event on 11 July than for the event on 9 June (Fig. 13d).

It is generally observed in the literature that hydrodynamic models do not perform well for low Froude numbers ($\mathrm{Fr} = v/\sqrt{gh}$). Hydrostatic models are instead appropriate for low Froude numbers ($\mathrm{Fr} < 1$), but underestimate forces for higher Froude numbers (Hübl *et al.*, 2009). The results obtained in this section appear to conform to this rule. A Froude number of about 0.7 was obtained for the event on 9 June, and of about 1.4 for event on 11 July. Accordingly, the event on 9 June is well described by a hydrostatic formula, while the event on 11 July is better described by the hydrodynamic formula.

Conclusions

The correct estimation of the impact force of a debris flow front against a mitigation structure is a key aspect in the structural design process, but it still remains an open issue. While numerous formulae are available for the evaluation of the impact force, these require the definition of empirical coefficients and a knowledge of the flow dynamics.

In this respect, the monitoring and measurement of real events is fundamental to gather reliable data concerning both flow dynamics and impact forces. To this end, a monitoring system equipped with strain transducers has been installed on the filter elements at the Grand Valey torrent study site. In this paper, we presented two debris flow events which occurred during the considered monitoring period. A video of the flow dynamics showing the interaction with the monitored barrier is available for the first of these two events.

The interpretation of the strain measurements in terms of the flow impact force requires the assumption of an impact load perpendicular to the barrier. This assumption is justified in the Grand Valey study site because of the existence of a narrow channel that forces the flow to impact orthogonally the monitored barrier, as was also observed in the video recordings. However, any upgrade of the system should include the installation of a second strain gauge at the lower left corner of the downstream side of each beam flange (i.e. in a symmetrical position to the existing instruments), in order to check the exact direction of the impact force of the debris flow. The lateral load, as shown in Leonardi & Pirulli (2020), can be significant if the outlets clog. Alternatively, load cells could be added to improve the characteristics of the existing monitoring system. A mounted camera that turns on during event would also significantly improve the site potential.

The video recordings give an important contribution to interpret both the debris flow dynamics and the strain gauge recordings, but also for the calibration of the rheological parameters used in numerical models. In the Grand Valey study site, the lack of a video for the second event made necessary to resort to the numerical modelling to obtain at least a rough estimation of the dynamics of the second event, using the rheological parameters obtained through the back analysis of the event on 9 July.

As far as the flow impact is concerned, forces, flow depth and velocity have been used to evaluate the applicability of the ranges of the empirical coefficients suggested in the literature. The obtained results highlight that hydrostatic effects dominated in the first event, while hydrodynamic effects dominated impact in the second event. For the Grand Valey site, both the static and the dynamic models should be applied: either of them can be more conservative, depending on the flow conditions. The maximum force obtained using formulae 4 and 5 should be selected as the design value. In order to be able to reproduce the force signal recorded on site, an empirical coefficient of at least 12 should be applied to both the static and dynamic formulas. However, the strains measured on site might be induced by a deformation pattern of the barrier than is more complex than the one assumed in our analysis. Thus, the derived empirical coefficient should be interpreted as conservative estimations.

Acknowledgements

This work was supported by the RISKNAT project - Operational programme Italy - France (Alps - ALCOTRA) 2007-2013, the “Mhymesis - Modelling Hazard of hYperconcentrated Mountain flows: a wEbgis SImulation System” project 2015-2017. The Authors wish to thank P. Gaia and L. Pitet (the Aosta Valley Autonomous Region) as well as M. Ceccarelli and A. Lombrino (Politecnico di Torino) for the configuration of the monitoring system and for suggestions for the interpretation of some of the monitoring data.

References

Arattano, M., Deganutti, A.M., and Marchi, L. 1997. Debris flow monitoring activities in an instrumented watershed on the Italian Alps. *In* Proceedings of 1st International Conference on Debris-Flow Hazards Mitigation. *Edited by* C. L. Chen, ASCE, New York, pp. 506–515.

Armanini, A., and Scotton, P. 1993. On the dynamic impact of a debris flow on structures. In Proceedings XXV IAHR Congress, Tokyo, Tech. Session B III, pp. 203-210.

Armanini, A. 1997. On the dynamic impact of debris flows. Recent developments on debris flows. Lecture notes in Earth Sciences. Springer Verlag Berlin, **64**: 208-226.

Audusse, E., Bristeau, M.O., and Perthame, B. 2000. Kinetic schemes for Saint-Venant equations with source terms on unstructured grids. Report 3989, Institut National de Recherche en Informatique et Automatique, LeChesnay, France, pp. 1-44.

Berti, M., Genevois, R., Simoni, A., and Tecca, P.R. 1999. Field observations of a debris flow event in the Dolomites. Geomorphology, **29**(3): 265–274.

Berger, C., McArdell, B.W., and Schlunegger, F. 2011. Direct measurement of channel erosion by debris flows, Illgraben, Switzerland. J Geophys Res Earth Surf, **116**: F01002.

Borri-Brunetto, M., Alessio, M., Barbero, M., Barpi, F., De Biagi, V., and Pallara, O. 2016. Stiffening effect of bolt-on transducers on strain measurements. Lat. Am. J. solids struct., 13(3): 536-553.

Canelli, L., Ferrero, A.M., Migliazza, M., and Segalini, A. 2012. Debris flow risk mitigation by the means of rigid and flexible barriers – Experimental tests and impact analysis. Nat Hazards Earth Syst Sci, **12**(5):1693–1699.

Coe, J.A., Kinner, D.A., and Godt, J.W. 2008. Initiation conditions for debris flows generated by runoff at Chalk Cliffs, central Colorado. Geomorphology, **96**(3–4):270–297.

Comiti, F., Marchi, L., Macconi, P., Arattano, M., Bertoldi, G., Borga, M., Brardinoni, F., Cavalli, M., D'Agostino, V., Penna, D., and Theule, J. 2014. A new monitoring station for debris flows in the European Alps: first observations in the Gadria basin. Nat Hazards, **73**(3):1175–1198.

Daido, A. 1993. Impact force of mud debris flows on structures. In Proceedings of XXV IAHR, Technical Session B, Debris Flow and Landslides, 3: 211-218.

Dowling, C.A., and Santi, P.M. 2014. Debris flows and their toll on human life: a global analysis of debris-flow fatalities from 1950 to 2011. Nat hazards, **71**(1):203–227.

Guzzetti, F., Stark, C.P., Salvati, P. 2005. Evaluation of flood and landslide risk to the population of Italy. J Environ Manag, **36**(1):15–36.

Hilker, N., Badoux A., and Hegg, C. 2009. The Swiss flood and landslide damage database 1972–2007. Nat Hazards Earth Syst Sci, **9**(3): 913–925.

Hu, K., Wei, F., Li, Y. 2011. Real-time measurement and preliminary analysis of debris-flow impact force at Jiangjia Ravine, China. Earth Surface Processes and Landforms, **36**(9):1268–1278.

Huang H.P., Yang K.C., and Lai S.W. 2007. Impact forces of debris flow on filter dam. Geophysical Research Abstracts, European Geosciences Union, Vol. 9, 03218.

Hübl, J., Suda, J., Moya, J., Proske, D., Kaitna, R., and Scheidl, C. 2009. Debris flow impact estimation. *In* Proceedings of the International Symposium on Water Management and Hydraulic Engineering. Ohrid (Macedonia), 1-5 September 2009, Paper A56, pp. 137–148.

Hürlimann, M., Rickenmann, D., and Graph, C. 2003. Field and monitoring data of debris-flow events in the Swiss Alps. Can Geotech J, **40**:161–175.

Hürlimann, M., Abancó, C., Moya, J., Raïmat, C., and Luis-Fonseca, R. 2011. Debris-flow monitoring stations in the Eastern Pyrenees. Description of instrumentation, first experiences and preliminary results. *In* Proceedings of 5th International Conference on Debris-Flow Hazards Mitigation. *Edited by* Genevois, R., Hamilton, D.L., and Prestininzi, A., Casa Editrice Università La Sapienza, Rome, pp. 553–562.

Hürlimann, M., McArdell, B.W., Rickli, C. 2015. Field and laboratory analysis of the runout characteristics of hillslope debris flows in Switzerland. Geomorphology, **232**: 20–32.

Iverson, R.M., and Denlinger, R.P. 2001. Flow of variably fluidized granular masses across three-dimensional terrain: 1. Coulomb mixture theory. J Geophys Res Solid Earth, **106**(B1):537–552.

Iverson, R.M., Logan, M., and Denlinger, R.P. 2004. Granular avalanches across irregular three-dimensional terrain. 2. Experimental tests. J Geophys Res, **109**(F1):F01015.

Iverson, R.M., Logan, M., LaHusen, R.G., and Berti, M. 2010. The perfect debris flow? Aggregated results from 28 large-scale experiments. J Geophys Res, **115**(F03005):29.

Jakob, M., Stein, D., and Ulmi, M. 2012. Vulnerability of buildings to debris flow impact. Nat Hazards, 60:241–261.

Kaitna, R., Proske, D., König, U., Hübl, J., and Holzinger, G. 2007. On design impact forces for torrential barrier structures. *In* Proceedings of 18thEuropean Safety and Reliability Conference, Stavanger, Norway, pp. 2209–2217.

Kogelnig, A., Hübl, J., Surinach, E., Vilajosana, I., and McArdell, B. 2014. Infrasound produced by debris flow: propagation and frequency content evolution. Nat Hazards, **70**(3):1713–1733.

Leonardi, A., Goodwin, G. R., and Pirulli, M. 2019. The force exerted by granular flows on slit dams. Acta Geotechnica, **14**(6): 1949–1963.

Leonardi, A., and Pirulli, M. 2020. Analysis of the load exerted by debris flows on filter barriers: Comparison between numerical results and field measurements. Computer & Geotechnics, **118**: 103311.

Lichtenhahn, C. 1973. Die Berechnung von Sperren in Beton und Eisenbeton. Kolloquium ü ber Wildbachsperren. Mitteilungen der Forstlichen Bundesanstalt Wien. Heft **102**:91–127.

Luis-Fonseca, R., Raïmat, C., Hürlimann, M., Abancó, C., Moya, J., and Fernández, J. 2011. Debris-flow protection in recurrent areas of the Pyrenees. Experience of the VX systems after the output results collected in the pioneer monitoring station in Spain. *In* Proceedings of 5th

International Conference on Debris-Flow Hazards Mitigation. *Edited by* Genevois, R., Hamilton, D., and Prestininzi A., Casa Editrice Università La Sapienza, Rome, pp. 1063–1071.

McDougall, S., & Hungr, O. 2005. Dynamic modelling of entrainment in rapid landslides. Canadian Geotechnical Journal, **42**(5): 1437–1448.

Marchelli, M., Leonardi, A., Pirulli, M., & Scavia, C. 2020. On the efficiency of slit dams in retaining granular flows. Géotechnique, in press.

Marchi, L., Arattano, M., and Deganutti, A.M. 2002. Ten years of debris-flow monitoring in the Moscardo Torrent (Italian Alps). Geomorphology, **46**(1):1–17.

McArdell, B.W., Bartelt, P., and Kowalski, J. 2007. Field observations of basal forces and fluid pore pressure in a debris flow. Geophys Res Lett, **34**(7).

McCoy, S.W., Kean, J.W., Coe, J.A., Staley, D.M., Wasklewicz, T.A., and Tucker, G.E. 2010. Evolution of a natural debris flow: in situ measurements of flow dynamics, video imagery, and terrestrial laser scanning. Geology, **38**:735–738.

Navratil, O., Liébault, F., Bellot, H., Theule, J., Travaglini, E., Ravanat, X., Ousse,t F., Laigle, D., Segel, V., and Fiquet, M. 2012. High-frequency monitoring of debris flows in the French Alps. *In* Proceedings of International Interpraevent Conference, Grenoble, France, pp. 281–291.

Navratil, O., Liébault, F., Bellot, H., Travaglini, E., Theule, J., Chambon, G., and Laigle, D. 2013. High-frequency monitoring of debris-flow propagation along the Réal Torrent, Southern French Prealps. Geomorphology, **201**: 157–171.

Okuda, S., Suwa, H., Okunishi, K., Yokoyama, K., and Nakano, M. 1980. Observations on the motion of a debris flow and its geomorphological effects. Z für Geomorphol Suppl **35**: 142–163.

Pierson, T.C. 1986. Flow behavior of channelized debris flows, Mount St. Helens, Washington. *In* Hillslope processes, *Edited by* Abrahms, A.D., Allen & Unwin, Boston, pp. 269–296.

Pirulli, M. 2005. Numerical modelling of landslide runout. A continuum mechanics approach. Ph.D. Thesis in Geotechnical Engineering, Department of Structural and Geotechnical Engineering, Politecnico di Torino, Italy.

Pirulli, M. 2010a. Morphology and substrate control on the dynamics of flowlike landslides J Geotech Geoenviron, **136**(2): 376-388.

Pirulli, M. 2010b. Chapter 4. Continuum Description of Flow-like Landslide Dynamics, *In* Continuum Mechanics, *Edited by* Andrus Koppel and Jaak Oja, Hauppauge, New York: Nova Science Publishers, Inc., pp. 105-146.

Pirulli, M. 2010c. On the use of the calibration-based approach for debris-flow forward-analyses. Natural Hazards and Earth System Sciences, 10: 1009-1019.

Pirulli, M. and Marco, F. 2010. Description and numerical modelling of the October 2000 Nora debris flow, Northwestern Italian Alps. Canadian Geotechnical Journal, **47**(2): 135-146.

Pirulli, M. and Pastor, M. 2012. Numerical study on the entrainment of bed material into rapid landslides. Geotechnique, **62**(11): 959-972.

Pirulli, M., Barbero, M., Barpi, F., Borri-Brunetto, M., and Pallara, O. 2014. The contribution of continuum mechanics based numerical models to design of debris flow barriers. *In* Proceedings of the 7th International Conference on Engineering Mechanics, Structures, Engineering Geology, June 3-5, Salerno, Italy, pp. 13-21.

Pitman, E.B., and Le, L. 2005. A two-fluid model for avalanche and debris flows. Philos T Roy Soc A, **363**(1832):1573–1601.

Pudasaini, S.P., Wang, Y., and Hutter, K. 2005. Modelling debris flows down general channels. Nat Hazards Earth Syst Sci, **5**(6): 799–819.

Revellino, P., Hungr, O., Guadagno, F.M., and Evans, S.G. 2004. Velocity and runout simulation of destructive debris flows and debris avalanches in pyroclastic deposits, Campania region, Italy. Environmental Geology, **45**: 295-311.

Rickenmann, D., and Koch, T. 1997. Comparison of debris flow modelling approaches, In: Proc. 1st Int. Conf. on Debris Flow Hazards Mitigation: Mechanics, Prediction, and Assessment, edited by: Chen, C.L., ASCE, Reston, Va., 576-585.

Rickenmann, D. 2005. Runout prediction methods. In Debris-flow Hazards and Related Phenomena, pp. 305–324. Springer.

Rickenmann, D., Laigle, D., McArdell, B.W., and Hübl, J. 2006. Comparison of 2D debris-flow simulation models with field events. Computational Geosciences, **10**: 241-264.

Suwa, H., Okano, K., and Kanno, T. 2011. Forty years of debris flow monitoring at Kamikamihorizawa Creek, Mount Yakedake, Japan. *In* Proceedings of 5th International Conference on Debris-Flow Hazards Mitigation. *Edited by* Genevois, R., Hamilton, D.L., and Prestininzi, A., Casa Editrice Università La Sapienza, Rome, pp. 605–613.

Tiranti, D., Crema, S., Cavalli, M., & Deangeli, C. 2018. An integrated study to evaluate debris flow hazard in alpine environment. Frontiers in Earth Science, **6**(May), 1–14.

Wendeler, C., McArdell, B.W., Rickenmann, D., Volkwein, A., Roth, A., and Denk, M. 2006. Field testing and numerical modelling of flexible debris flow barriers. *In* Proceedings of 6thInternational Conference of Physical Modelling in Geotechnics. *Edited by* Ng, C.W.W., Zhang, L.M., and Wang, Y.H., CRC Press, Hong Kong, pp. 1573–1604,

Yin, H.Y., Huang, C.J., Chen, C.Y., Fang, Y.M., Lee, B.J., and Chou, T.Y. 2011. The present development of debris flow monitoring technology in Taiwan-a case study presentation. *In* Proceedings of 5th International Conference on Debris-Flow Hazards Mitigation. *Edited by* Genevois, R., Hamilton, D.L., and Prestininzi, A., Casa Editrice Università La Sapienza, Rome, pp. 623–631.

Zhang, S. 1993. A comprehensive approach to the observation and prevention of debris flows in China. Nat Hazards, **7**(1):1–23.

Figures

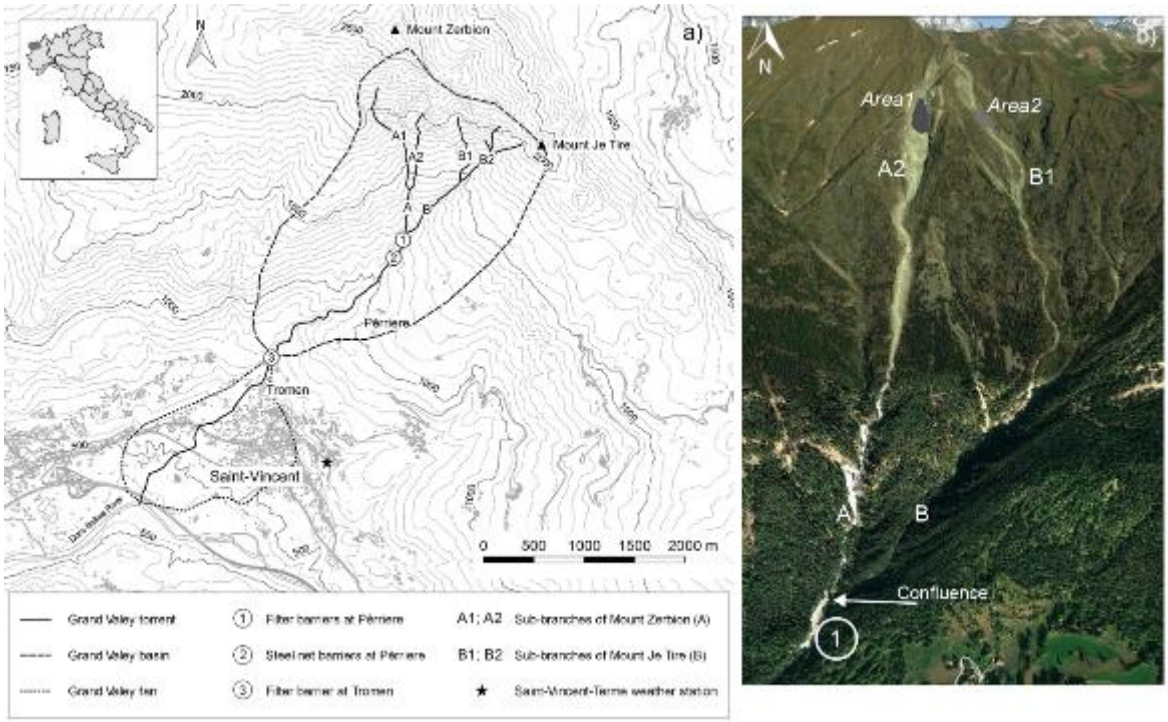

Fig. 1 (a) Location and main characteristics of the Grand Valey basin; (b) details of the two most actives sub-branches (A2, B1), with indication of their confluence upstream of the filter barriers at Pèrriere. *Area 1* and *Area 2* identify the main areas prone to originating flow instabilities. Modified after Leonardi & Pirulli (2020).

Fig. 2 The structural mitigation works along the Grand Valey torrent: (a) the two filter barriers at the Pèrriere hamlet; (b) the steel net barriers; (c) the slit-filter barrier at Tromen; (d) the barrier at Pèrriere (white rectangle in Fig. 2a) that collapsed in 2014. The position of each of these structures is indicated in Fig. 1 (photos courtesy of the Aosta Valley Autonomous Region).

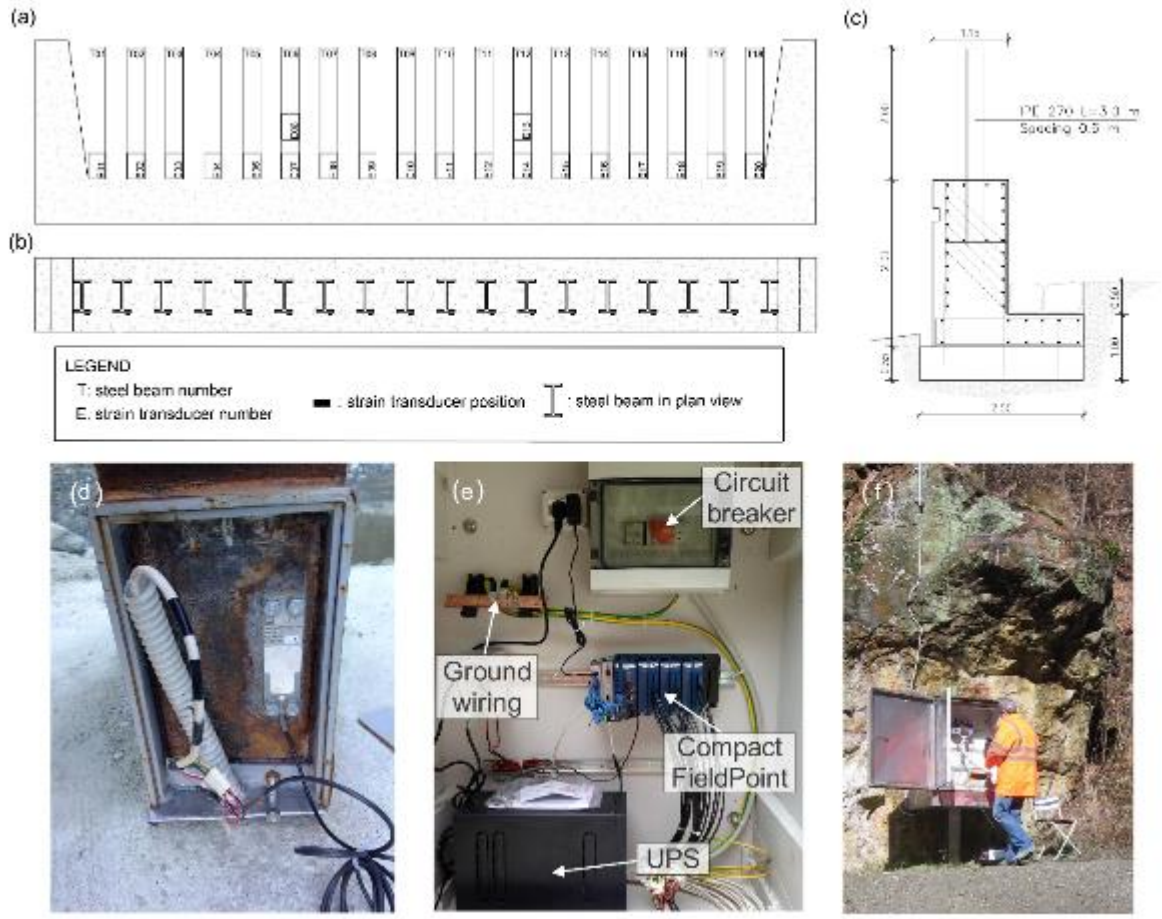

Fig. 3 The monitored filter barrier. (a) front and (b) plan views from below, with indications of the positions of the strain gauges (E) (not to scale); (c) the cross section (dimensions in metres); (d) open protective steel box, with the positions of the transducers; (e) controller system components; (f) waterproof container protected by a stainless-steel locker.

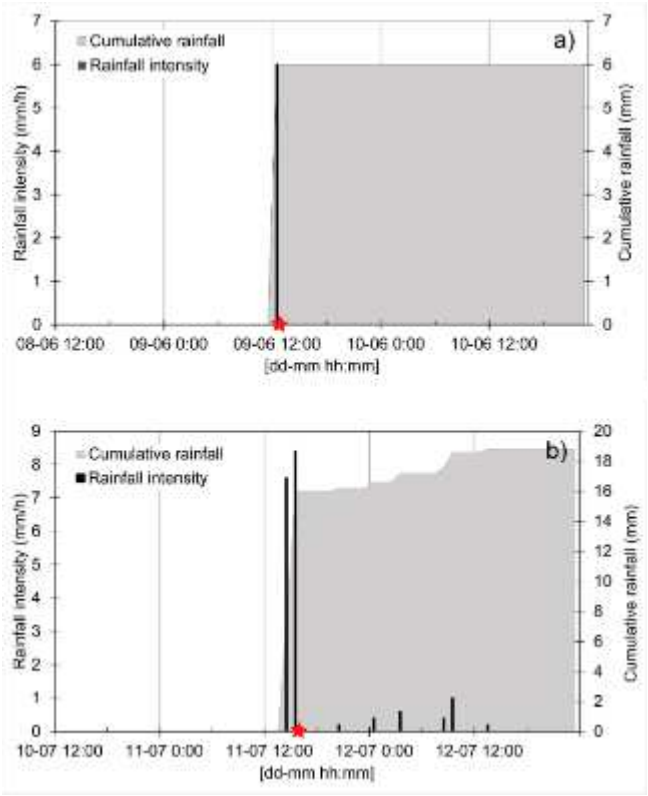

Fig. 4 Rainfall data recorded at the Saint-Vincent Terme weather-station referring to when the debris flow on (a) 9 June and (b) 11 July occurred. The red markers point the exact time when the debris flows occurred.

Fig. 5 A portion of the vertical longitudinal trench through the central part of the deposit of the event on 9 June.

Fig. 6 The deposit of the event of 11 July.

Fig. 7 Event on 9 June: (a) the frontal part of the debris flow at the confluence between branches A and B; (b) the asymmetric dynamics of the flow. The bold line defines the limit between the fluid- and the coarse part of the flowing mass; (c)-(d) the interaction of the mass with the monitored barrier at two consecutive moments.

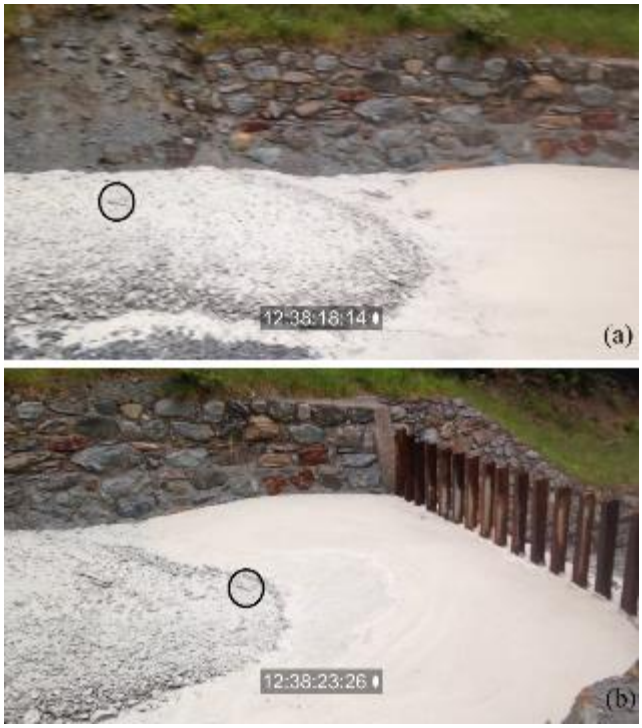

Fig. 8 Event on 9 June: Example of particle-motion tracking as the video advances frame-by-frame. Note that before hitting the barrier, the front submerges into a pool of water accumulated behind the barrier, becoming undetectable. Therefore, we use the last available frames with a visible front for the particle tracking procedure.

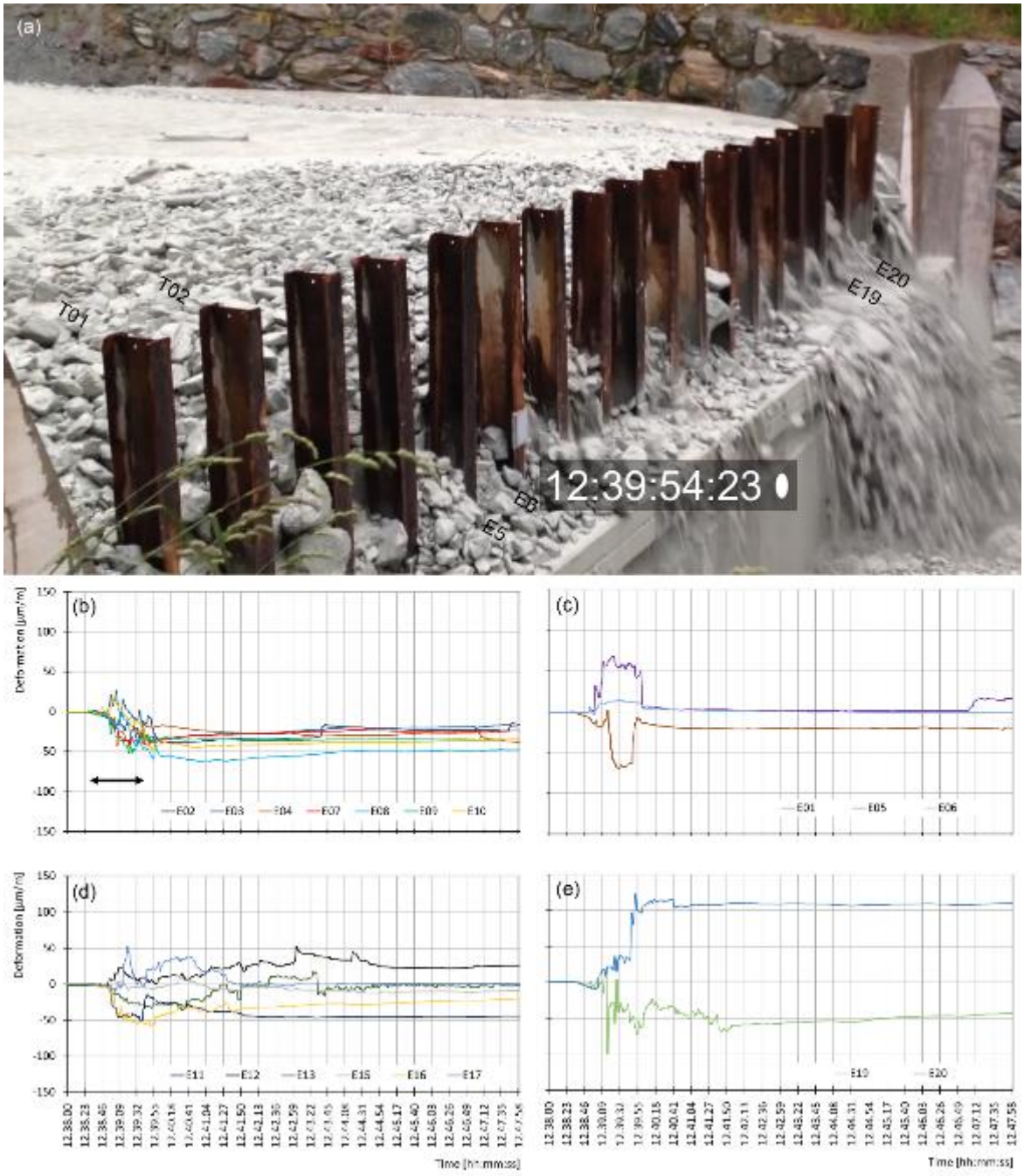

Fig. 9 Strain measurements recordings for the event on 9 June. (a) distribution of the deposit upstream of the monitored barrier; (b) and (c) data collected from E01 to E10 (i.e. the right side of the barrier), while (d) and (e) concern data from E11 to E20 (i.e. the left side of the barrier). The horizontal black arrow indicates the time interval in which compression (negative strain) increases.

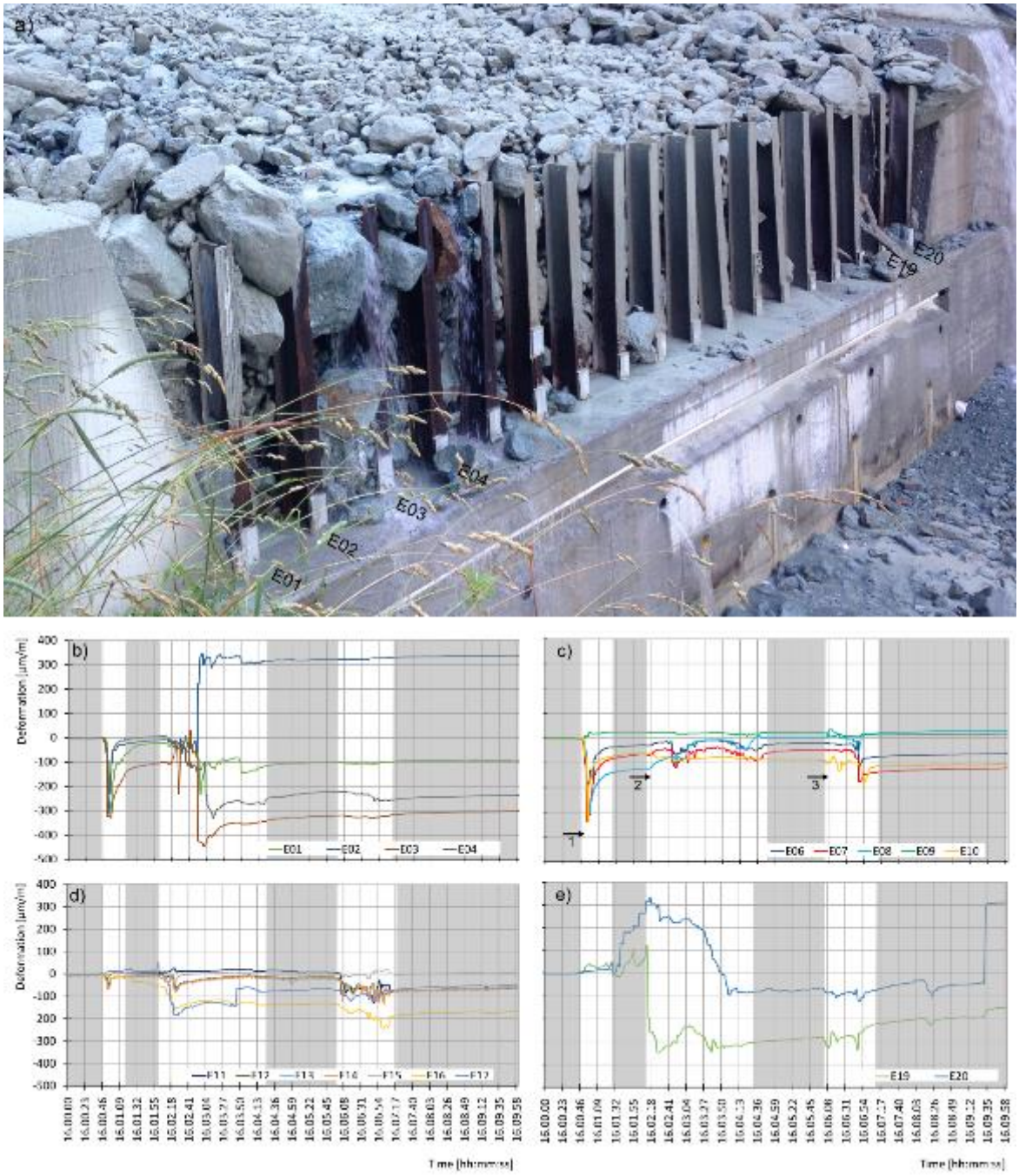

Fig. 10 Strain measurements for the event on 11 July. (a) distribution of the deposit; (b) and (c) collected from E01 to E10 (i.e. the right side of the barrier), while (d) and (e) concern data from E11 to E20 (i.e. the left side of the barrier). The black arrows in (c) give a rough indication of the initiation of each flow surge. The shaded areas indicate the time interval in which the measured strain remain roughly constant.

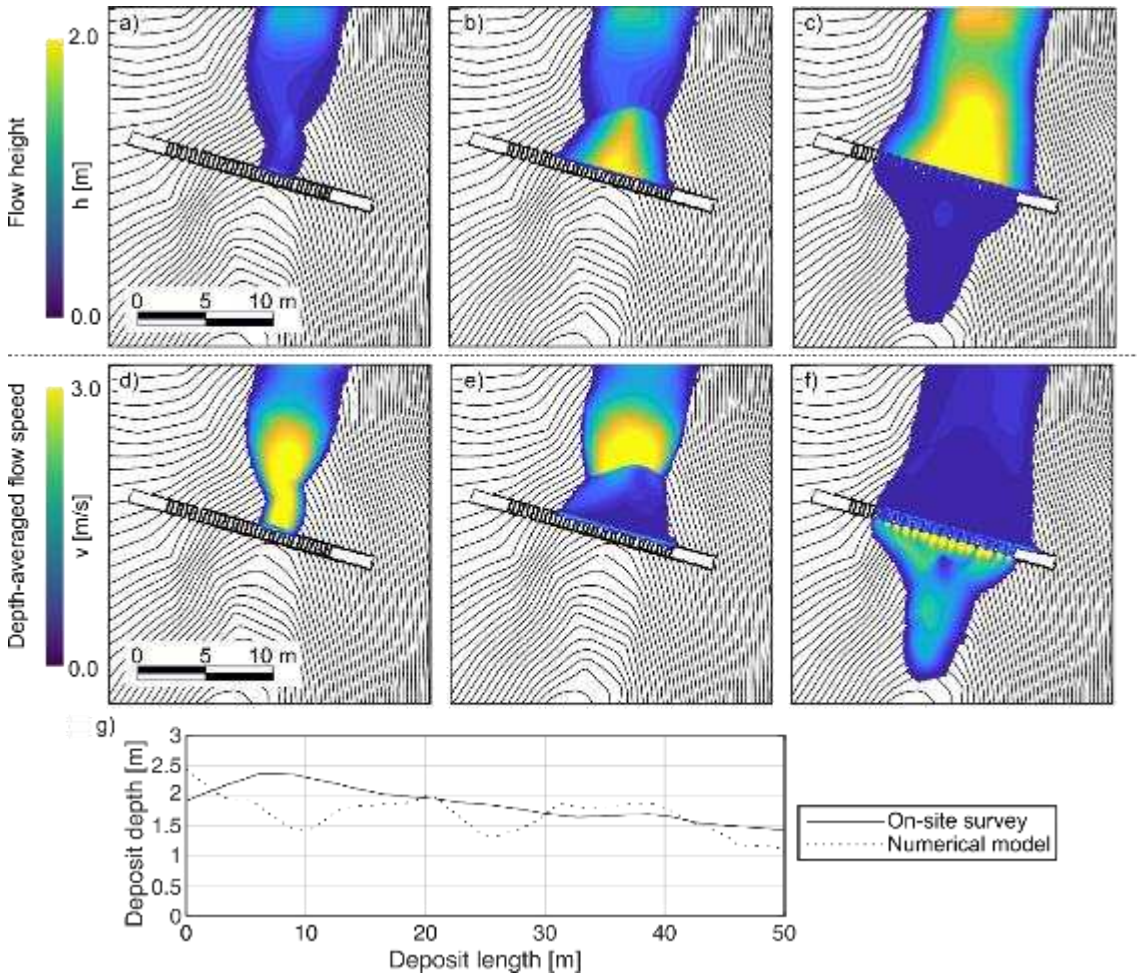

Fig. 11 Numerical modelling of the event on 9 June with the calibrated Voellmy rheology. Flow height: (a) at impact; (b) when the barrier is first overtop; (c) when the flow filters through the openings. The depth-averaged speed at the same instants is shown in panels (d-f): Final deposit: (g) longitudinal profile from the barrier toward upstream with respect to the onsite surveyed profile, see Fig. 5.

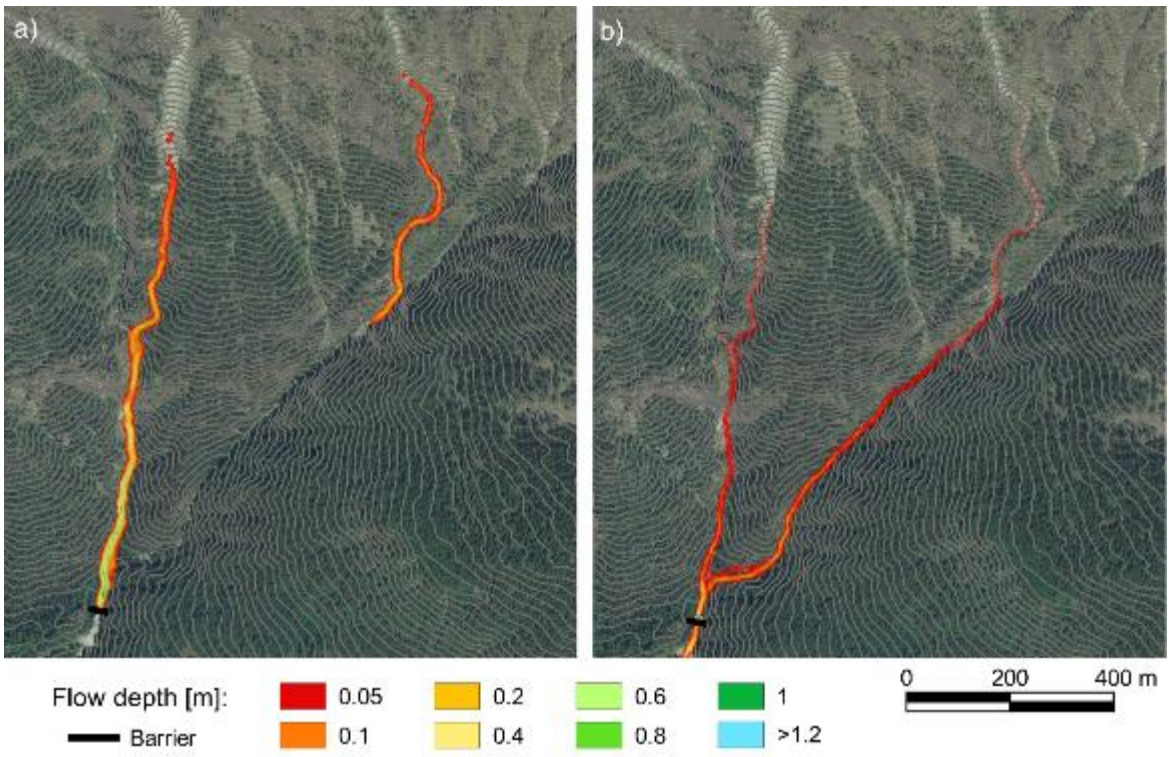

Fig. 12 Modelling of the event on 11 July with the calibrated Voellmy rheology: (a) 195 s, (b) 500 s.

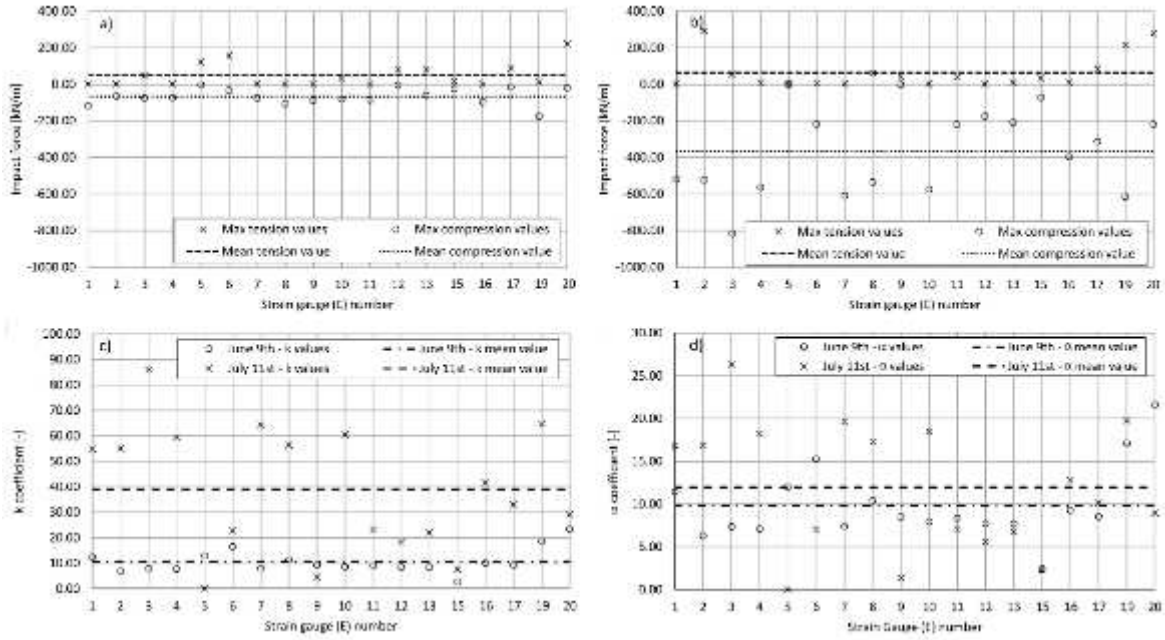

Fig. 13 Impact force calculated from the strain measurements: (a) for the event on 9 June and (b) for the event on 11 July. Estimation of values of the empirical coefficients: (c) static coefficient k and (d) dynamic coefficient α.

Tables

Table 1 Main morphological features.

Grand Valey basin		
Maximum altitude	2681	m
Minimum altitude	680	m
Mean altitude	1466	m
Area	5.22	km^2
Mean slope	82	%
Grand Valey fan		
Maximum altitude	680	m
Minimum altitude	445	m
Area	1.47	km^2
Grand Valey torrent		
Length of the main channel	5.71	km
Length of the main channel in the drainage basin	3.76	km
Length of the main channel on the fan	1.95	km
Total length of secondary channels	14.76	km
Mean slope of the main channel	38	%
Mean slope of the main channel on the fan	12	%
Mean slope of the channel	29	%

Table 2 List of the main documented debris flow events at Grand Valey (dates are given in DD/MM format).

2004		**2008**		**2009**	
Date	Volume [m^3]	Date	Volume [m^3]	Date	Volume [m^3]
07/08	3000	28/05	6400	26/05	10000
		12/07	3500		
		06/09	5000		
		03/11	3000		

2011		**2012**		**2013**	
Date	Volume [m^3]	Date	Volume [m^3]	Date	Volume [m^3]
06/06	3975	29/08	3975	17/07	3550
16/06	200			29/07	3810
17/06	300				
22/06	500				
13/07	4500				
26/08	4500				

2014		**2015**		**2016**	
Date	Volume [m^3]	Date	Volume [m^3]	Date	Volume [m^3]
06/06	2790	19/03	800	09/06	1875
12/06	2090	08/06	5000	11/07	4420
07/07	4670	14/08	2000		
20/07	4625				
23/07	2565				
03/08	725				

Table 3 Debris flow on 9 June: dimensions of the main deposit.

Main deposit plan view		
Maximum front width	18	m
Minimum rear width	10	m
Average length	80	m
Average area	1100	m^2
Main deposit longitudinal profile		
Front average depth	2	m
Centre average depth	1.6	m
Rear average depth	0.8	m

Table 4 Event on 9 June: Particle tracking of some debris selected for the front velocity estimation before impact.

Particle reference	Time interval [s]	Distance [m]	Estimated velocity [m/s]
1	4.3	8.3	2.0
2	5.6	14.8	2.6
3	5.3	11.4	2.2
4	4.2	10.0	2.4
5	5.0	12.2	2.5
6	4.1	9.1	2.2
7	4.1	9.5	2.3
8	4.7	10.4	2.3

Table 5 Debris flow on 9 June: Comparison between data of the observed and simulated velocity and flow depth. $\bar{v}$: mean velocity of the mass front between the confluence of branches A and B to the barrier; $\overline{h}$: mean depth of the frontal part of the deposit; $\bar{l}$: mean length of the main deposit.

Simulation results				
Voellmy rheology		$\bar{v}$ **[m/s]**	$\overline{h}$ **[m]**	$\bar{l}$ **[m]**
μ [-]	**ξ [m/s²]**			
0.1	1000	5.3	2.3	30
	500	4.0	2.4	31
	300	3.2	2.7	36
	200	2.7	2.8	36
0.2	1000	2.7	2.7	85
	500	2.0	2.4	82
	400	1.6	2.2	81